Ab initio theory of the N_2V defect in diamond for quantum memory implementation

Péter Udvarhelyi,[1,2] Gergő Thiering,[2,3] Elisa Londero,[2] and Adam Gali[2,3,*]
[1]*Loránd Eötvös University, Pázmány Péter Sétány 1/A, H-1117 Budapest, Hungary*
[2]*Wigner Research Centre for Physics, Hungarian Academy of Sciences, P.O. Box 49, H-1525 Budapest, Hungary*
[3]*Budapest University of Technology and Economics, Budafoki út 8, H-1111 Budapest, Hungary*

(Received 25 April 2017; revised manuscript received 18 August 2017; published 30 October 2017)

The N_2V defect in diamond is characterized by means of *ab initio* methods relying on density functional theory calculated parameters of a Hubbard model Hamiltonian. It is shown that this approach appropriately describes the energy levels of correlated excited states induced by this defect. By determining its critical magneto-optical parameters, we propose to realize a long-living quantum memory by N_2V defect, i.e., $H3$ color center in diamond.

DOI: 10.1103/PhysRevB.96.155211

I. INTRODUCTION

Paramagnetic point defects in diamond are candidates for quantum bit and quantum information applications. Various defects were identified as optically active color centers [1]; most notable is the nitrogen-vacancy (NV) [2]. NV is formed in diamond by the trapping of a mobile vacancy by the substitutional nitrogen atom. In nitrogen rich diamond aggregation of substitutional nitrogen atoms may occur. The neighbor substitutional nitrogen pair is an example for such aggregation (A aggregate). Similar to the NV defect, the N_2V defect is formed by an A aggregate trapping a mobile vacancy [3]. Uniaxial stress measurements already established the N-V-N structure of the N_2V defect with C_{2V} symmetry [see Fig. 1(a)] [4]. The effective one-electron picture of the defect is described by Lowther [5]. The defect in its neutral charge state was assigned to $H3$ color center [6] with a zero-phonon line (ZPL) of 2.463 eV, where this signal was associated with the optical transition between $^1A_1$ ground and $^1B_1$ excited states [7]. The $H3$ photoluminescence (PL) center has a PL lifetime of 17.5 ns and an outstanding 0.95 quantum yield [8] that makes the defect a stable single-photon source [9]. An optically inactive $^1A_1$ state with an absorption line at 2.479 eV was revealed under uniaxial stress measurements [7]. Furthermore, an $H13$ absorption band with ZPL at 3.364 eV was also observed and interpreted as a transition to higher excited states [10]. The $H3$ center shows delayed luminescence, that was interpreted as a reversible transition from the $^1B_1$ excited state to metastable triplet states, with radiative decay time in the order of tens of milliseconds [11]. Its paramagnetic metastable triplet state was investigated by electron-spin resonance (ESR) spectroscopy, called W26 center, under illumination at room temperature. The experimental zero-field splitting (ZFS) tensor principal values are $D_{xx} = 1.43$ GHz and $D_{zz} = -2.63$ GHz. The measured hyperfine parameters of ^{14}N nuclei are $A_\perp = 10.2$ MHz and $A_\parallel = 21.5$ MHz [12].

Our study is motivated by the success of optically detected magnetic resonance (ODMR) applications of a single NV defect [13] and the readout and control of single nuclear spin with ST1 ODMR center in diamond [14]. The latter employs optical pumping to metastable triplet state where initialization of the nuclear spin is achieved by spin-polarization transfer exploiting the hyperfine level anticrossing (LAC). As the metastable triplet state relaxes to the singlet ground state, the nuclear-spin coherence time is not reduced by the persistent electron spin. As the $H3$ center exhibits a singlet ground state and an optically accessible metastable triplet state we wished to explore the properties of the N_2V defect for quantum memory applications.

To this end, we characterize this defect in diamond by means of advanced density functional theory (DFT) calculations. In this paper, we demonstrate that optical spin polarization of the triplet state and spin polarization transfer to the existing nuclear spins is principally feasible, i.e., a long-living quantum memory may be realized with N_2V defect. Their magneto-optical parameters are determined by means of DFT calculations that go beyond the conventional Kohn-Sham DFT methods. By combining von Barth theory [15] and the Hubbard model we developed an *ab initio* method to calculate the energy of highly correlated multiplets using only Kohn-Sham DFT wave function and energies, and we apply this to the neutral N_2V defect.

We organized our paper as follows. In the next section (Sec. II), details about the computational method are given including test results on the negatively charged N_2V defect. We focus then on the proposed quantum memory application of the neutral N_2V defect in Sec. III that is the main topic of our paper. In Sec. IV we describe the Hubbard Hamiltonian analysis of the electronic structure of the neutral N_2V defect. We report the calculated *ab initio* magneto-optical parameters in Sec. V that are taken in the quantum memory discussion in Sec. III.

II. COMPUTATIONAL METHOD

We carried out DFT calculations for electronic structure calculation and geometry optimization within the spin-polarized HSE06 hybrid functional [16] using the plane-wave and projector augmented-wave (PAW) formalism based Vienna Ab initio Simulation Package (VASP) [17–21]. The model of N_2V in bulk diamond was constructed using a 512-atom diamond simple cubic supercell within the Γ-point approximation. The Γ-point approximation simplifies the process of ensuring the proper symmetry of the Kohn-Sham wave functions which is advantageous in our method. The Γ-point sampling of the

---

[*] gali.adam@wigner.mta.hu

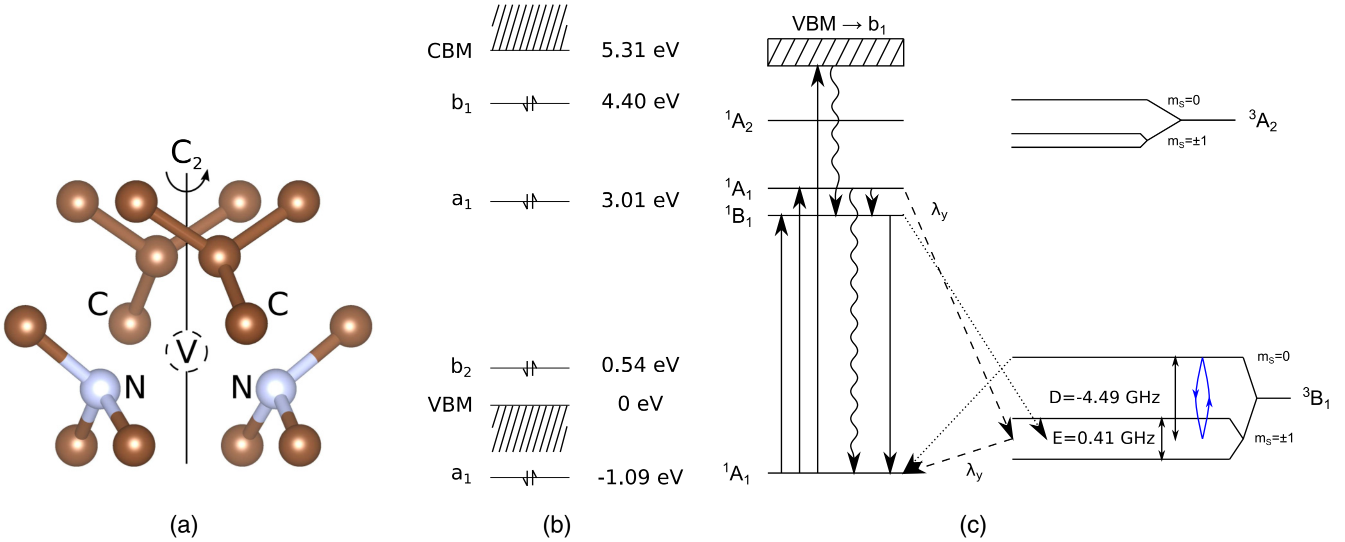

FIG. 1. (a) Geometry of N_2V defect in diamond. (b) Representation of defect levels of double negatively charged N_2V with closed-shell orbitals relative to the valence-band maximum (VBM). (c) Analysis of ODMR contrast of the neutral N_2V. Straight line illustrates radiative decay, dashed and dotted lines represent ISC with first-order and second-order spin-orbit couplings (λ), respectively. Curved lines and blue arrows indicate phonon and microwave transition, respectively. The calculated zero-field splitting parameters are given for ${}^3B_1$ state at 0 K temperature.

Brillouin zone has proven sufficient for various defects in diamond for 512-atom supercell [22,23]. This implies that the employed parameters provide sufficiently converged results for N_2V. Most of the calculations were performed with 370-eV plane-wave cutoff energy that is sufficient for electronic structure of nitrogen-vacancy-type defect calculations [22]. Hyperfine interaction parameters were obtained with core correction included [24] with an increased cutoff energy of 500 eV. Zero-field splitting parameters were calculated with a home-built code with the use of the same parameters and methods that are given in Ref. [25].

The HSE06 calculations provide excellent results for the negatively charged N_2V defect which has a spin doublet with no high correlation between the electron states. To demonstrate this, we compare the experimental hyperfine constants [26] with our HSE06 DFT calculations in Table I, and we found excellent agreement. This supports applying the HSE06 functional for orbitals that are not highly correlated. However, we found that the neutral N_2V is very challenging for Kohn-Sham DFT functionals because of the highly correlated open-shell orbitals. We present a method in Sec. IV that properly calculates these states that involves a Hubbard model Hamiltonian. Our method can be useful in the study of other quantum bits with highly correlated electronic states.

TABLE I. HSE06 DFT calculated and experimental (in parentheses) hyperfine principal values for the first-neighbor nitrogen and first carbon atoms around the vacancy of the negatively charged N_2V defect. The experimental data are taken from Ref. [26].

Atom	A_{xx} (MHz)	A_{yy} (MHz)	A_{zz} (MHz)
^{15}N	4.0 (3.47)	4.5 (4.09)	5.0 (4.51)
^{13}C	190.8 (202.3)	191.6 (202.3)	314.3 (317.5)

III. PROPOSED QUANTUM MEMORY APPLICATION OF THE N_2V DEFECT

By using HSE06 we found in an earlier study [22] that the $(+|0)$ and $(0|-)$ charge transition levels of N_2V defect are at $E_C - 4.8$ eV and $E_V + 3.3$ eV, respectively, where E_C and E_V are the conduction- and valence-band edges, respectively. This explains the stability of its neutral charge state at various doping concentrations. Furthermore, its H13 absorption band can be associated with the transitions from the valence band to the empty in-gap defect level of the neutral defect. The method to calculate the lower energy states and electronic structure is given in the next sections. Our basic results are summarized in Fig. 1, which shows the optically induced electron spin-polarization process. We find two optically active excited states (${}^1B_1$ and ${}^1A_1$ with small energy gap) and an optically forbidden dark state (${}^1A_2$). After the excitation to the phonon sideband of the optically allowed singlet excited states, it can relax to the vibronic ground state of ${}^1B_1$, and then back to the ${}^1A_1$ electronic ground state with emitting a photon. Alternatively, intersystem crossing (ISC) from ${}^1B_1$ to ${}^3B_1$ may take place too as a second-order process, where mixing of the excited ${}^1B_1$ and ${}^1A_1$ states caused by B_1-type phonons makes the intersystem crossing feasible via spin-orbit interaction. At elevated temperatures, the ${}^1A_1$ excited state may be thermally occupied (experimental gap is 16 meV in Ref. [7]) and then a first-order ISC to ${}^3B_1$ can occur. This is a *spin selective* transition to $m_S = \pm 1$ as only λ_y of B_1 symmetry can couple these states, where λ_y is the y component of the spin-orbit coupling. We note that the spin sublevels of the triplet split even at zero magnetic field that is caused by the electron-spin–electron-spin dipolar interaction (zero-field splitting) because of the low-symmetry crystal field. Thus, the spin selective ISC will indeed populate only the $m_S = \pm 1$ states. From this metastable triplet, an ISC can occur to the singlet ground state. Again, the transition from the triplet $m_S = \pm 1$ and $m_S = 0$

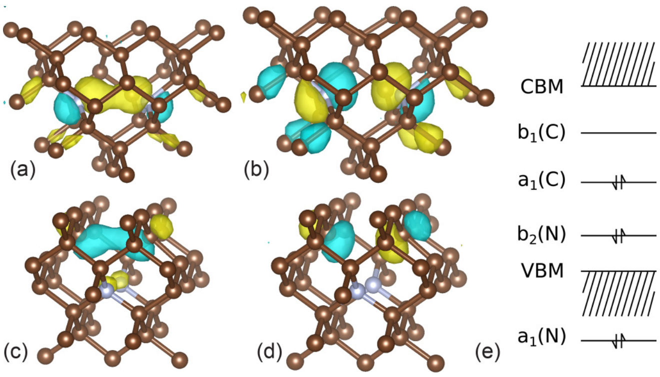

FIG. 2. Visualization of geometric structure and defect wave functions of N_2V. Brown and blue balls represent the carbon and nitrogen atoms, respectively. Defect states are labeled by their irreducible representation and localization. (a) a_1(N), (b) b_2(N), (c) a_1(C), (d) b_1(C), (e) defect levels.

substates to the singlet ${}^1A_1$ ground state is a first-order and a second-order process, respectively, because of the selection rules. The singlet-triplet ISC is expected to be significantly slower than the rate of the radiative decay, because of the large gap between the excited-state singlet and the metastable triplet according to our *ab initio* result. This is in contrast to the interpretation of an experiment [11] that we will discuss below. This *ab initio* result may explain the large quantum yield of the defect. In the optical cycle, ODMR contrast can be achieved by microwave excitation, owing to the lifetime differences of first- and second-order transitions from the different triplet substates to the singlet ground state.

The system shows characteristics that makes it a promising candidate for quantum memory applications. Electron spin polarization can be achieved in the ODMR cycle by populating the $m_S = \pm 1$ sublevel of the metastable triplet. The ^{14}N (or ^{15}N nuclei of the defect and ^{13}C nuclei in their vicinity are candidates for quantum memory. The calculated hyperfine constants are listed for these nuclear spins in Sec. V. Spin-polarization transfer between electron and nearby nuclear spins can be realized at the LAC condition by optical pumping of the defect (see a detailed analysis of this process in Refs. [27,28]). LAC condition can be realized by a constant external magnetic field which is perfectly aligned with the symmetry axis of the defect and its magnitude equals the zero-field splitting [14,29]. After the nuclear spin was set, the electron will naturally decay to the singlet ground state that does not decohere the nuclear spin.

IV. HUBBARD MODEL OF THE ELECTRONIC STATES

Next, we discuss the nature of electronic structure of the neutral N_2V and methods to calculate it properly. The four dangling bonds of the defect under C_{2v} symmetry produces b_2, a_1, and b_1 Kohn-Sham levels in the gap, in ascending energy order (see Fig. 2), that may be derived from a split t_2 state of the vacancy. In addition, another a_1 forms resonant with the valence band. These states are occupied by six electrons. The highest energy occupied in-gap a_1 state (HOMO) is a stretched C-C bonding state while the lowest energy empty b_1 state (LUMO) is a C-C antibonding state [30]. As we will show below, HSE06 DFT calculations cannot describe the various multiplet states of the defect caused by the strong correlation of open-shell orbitals. In the following we will use a Hubbard model Hamiltonian to represent the strongly correlating electrons. We particularly focus on the HOMO a_1 and LUMO b_1 states as active space for the correlated electrons that contribute to the lowest energy excitation configurations.

Our active space with a_1 and b_1 states may be labeled simply a and b, respectively. Then these states may be given as $a = \frac{1}{\sqrt{2}}(A + B)$ and $b = \frac{1}{\sqrt{2}}(A - B)$ where A and B are dangling bonds on the two nearest-neighbor carbon atoms. The singlet determinants with A_1 symmetry are $|{}^1A_{1(g)}\rangle = |a^{\uparrow}a^{\downarrow}\rangle$, $|{}^1A_{1(e)}\rangle = |b^{\uparrow}b^{\downarrow}\rangle$, $|{}^1B_1\rangle = \frac{1}{\sqrt{2}}(|a^{\uparrow}b^{\downarrow}\rangle - |a^{\downarrow}b^{\uparrow}\rangle)$. The triplet determinants are $|{}^3B_1\rangle = |a^{\uparrow}b^{\uparrow}\rangle$; $|a^{\downarrow}b^{\downarrow}\rangle$ for $m_S = \pm 1$, respectively, and $|{}^3B_1\rangle = \frac{1}{\sqrt{2}}(|a^{\uparrow}b^{\downarrow}\rangle + |a^{\downarrow}b^{\uparrow}\rangle)$ for $m_S = 0$. Substituting a and b in the above formulas, the atomic-orbital form of the determinants can be obtained. The electronic structure of the neutral N_2V defect can be described by a Hamilton operator derived from configurational interaction with zero differential overlap (ZDO) approximation and Heisenberg spin coupling. The full Hamiltonian then can be described as a Hamiltonian familiar with the Hubbard model [31] ($\hat{H}'$) plus the Hamiltonian of the bath of weakly interacting electrons ($\hat{H}_0$)

$$\begin{aligned}
\hat{H} &= \hat{H}' + \hat{H}_0 \\
&= U(\hat{n}_{A\uparrow}\hat{n}_{A\downarrow} + \hat{n}_{B\uparrow}\hat{n}_{B\downarrow}) \\
&\quad - \frac{t}{4}(\hat{c}^{\dagger}_{A\uparrow}\hat{c}_{B\uparrow} + \hat{c}^{\dagger}_{A\downarrow}\hat{c}_{B\downarrow} + \hat{c}^{\dagger}_{B\uparrow}\hat{c}_{A\uparrow} + \hat{c}^{\dagger}_{B\downarrow}\hat{c}_{A\downarrow}) \\
&\quad + C(\hat{n}_{A\uparrow}\hat{n}_{B\uparrow} + \hat{n}_{A\downarrow}\hat{n}_{B\downarrow} + \hat{n}_{A\uparrow}\hat{n}_{B\downarrow} + \hat{n}_{A\downarrow}\hat{n}_{B\uparrow}) \\
&\quad - 2J(\hat{c}^{\dagger}_{A\uparrow}\hat{c}_{A\downarrow}\hat{c}^{\dagger}_{B\downarrow}\hat{c}_{B\uparrow} + \hat{c}^{\dagger}_{A\downarrow}\hat{c}_{A\uparrow}\hat{c}^{\dagger}_{B\uparrow}\hat{c}_{B\downarrow}) \\
&\quad - J(\hat{n}_{A\uparrow}\hat{n}_{B\uparrow} + \hat{n}_{A\downarrow}\hat{n}_{B\downarrow} - \hat{n}_{A\downarrow}\hat{n}_{B\uparrow} - \hat{n}_{A\uparrow}\hat{n}_{B\downarrow}) + \hat{H}_0,
\end{aligned} \tag{1}$$

where the first term is the on-site repulsion, the second is the hopping, the third is the Coulomb repulsion, and the last two terms in $\hat{H}'$ are from the Heisenberg exchange interaction in the Hubbard Hamiltonian. $\hat{n}$ is the particle number operator while $\hat{c}^{\dagger}$ and $\hat{c}$ is the creation and annihilation operators, respectively. The eigenvalue of H_0 is E_0 that is the total energy of the bath of weakly interacting electrons that should be added to the solution of $\hat{H}'$. We use the symmetry adapted basis above to write down the matrix of the $\hat{H}'$ Hubbard Hamilton operator,

$$H' = \begin{array}{c}
\begin{array}{cccc} |{}^1A_{1(g)}\rangle & |{}^1A_{1(e)}\rangle & |{}^1B_1\rangle & |{}^3B_1\rangle \end{array} \\
\left(\begin{array}{cccc}
\frac{U-t+C+3J}{2} & \frac{U-C-3J}{2} & & \\
\frac{U-C-3J}{2} & \frac{U+t+C+3J}{2} & & \\
 & & U & \\
 & & & C-J
\end{array}\right)
\end{array}, \tag{2}$$

where we neglected the zero-field splitting in the ${}^3B_1$ state. In the HSE06 DFT functional calculations the off-diagonal terms are completely neglected, with resulting in Ψ_1 and Ψ_3 states with ${}^1A_1$ symmetry. The ${}^1B_1$ state is a multideterminant state, and HSE06 DFT cannot calculate the true eigenstate or, as a consequence, the true eigenenergy of the system. Instead, one can calculate

$$E(\Psi_2) = \langle a^{\uparrow}b^{\downarrow}|H|a^{\uparrow}b^{\downarrow}\rangle = \frac{U + C - J}{2} + E_0. \tag{3}$$

Finally, one can calculate the HSE06 DFT total energies for Ψ_1, Ψ_3, ${}^3B_1$ [corresponding diagonal terms in Eq. (2)] and for Ψ_2 [Eq. (3)], that provides four equations for the full Hamiltonian parameters. In the full Hamiltonian there are five parameters, however, we are interested in the excitation energies for which three combined parameters, t, J, and $U-C$, are left [see Eqs. (A5)–(A7) in Appendix A] that can be derived from the total-energy expressions of Ψ_{1-3} and ${}^3B_1$.

The HSE06 DFT total energies for these various states can by obtained by ΔSCF calculations [32]. In order to work with a “noncorrelated” basis for ΔSCF energy calculations required in the Hubbard Hamiltonian, we used the basis functions of the closed-shell system of the defect in its double negatively charged state N_2V [Fig. 1(b)], calculated in the N_2V^0 ground-state geometry. This choice provides a basis that is free from spin contamination and strong correlation effects. We note that the relaxed orbitals within unrestricted spin-polarized DFT Kohn-Sham formalism result in lower total energies (see Appendix B). However, our main purpose here is to calculate the excitation energies. As the same restriction on the Kohn-Sham orbitals applies in all the electronic configurations (ground state and excited states), we implicitly assumed that this restriction has the same effect for all the electronic configurations. Finally, the calculated excitation energies are in order.

Another basis that prevents spin contamination could be the neutral state with partially occupied defect levels. However, these basis functions cannot prevent strong correlation effects via Coulomb interaction because of the open-shell electronic structure. We conclude that the only proper basis is to select the Kohn-Sham wave functions (orbitals) from the closed shell (2−) charge state. The total energies in the various occupation of Kohn-Sham states representing the Ψ_1, Ψ_2, Ψ_3, ${}^3B_1$ multiplets were calculated by keeping these orbitals fixed. We note that this procedure is very different from the usual self-consistent unrestricted spin-polarized DFT method. Consequently, the two approaches result in different excitation energies by the ΔSCF method (see Appendix B). Our procedure with fixed orbitals guarantees the proper spin state and symmetry of the single determinant many-body state.

By calculating the HSE06 DFT energies for the Ψ_{1-3} and ${}^3B_1$ states (summarized in Table II), the parameters in the Hubbard Hamiltonian can be calculated *ab initio*, and the resultant values are $t = 2.23$ eV, $U - C = 2.05$ eV, and $J = 0.05$ eV, respectively. The singlet-triplet coupling is minor, and the $U-C$ terms and the hopping term t dominate, $U - C \approx t \approx 2$ eV. A very important finding is that the calculated $\Psi_1 \to \Psi_2$ excitation energy by the self-consistent spin-polarized DFT method scales up by $\approx 1+\sqrt{2}/2 \approx 1.7$, with respect to the the correct ${}^1A_{1(g)} \to {}^1B_1$ excitation energy obtained by the Hubbard model. In other words, the vertical excitation energy associated with the ${}^1B_1$ state increases in the order of eV in the Hubbard model with respect to the HSE06 Kohn-Sham DFT result. As a consequence, the excitation energies of the ${}^1A_{1(g)} \to {}^1B_1$ and ${}^1A_{1(g)} \to {}^1A_{1(e)}$ transitions are close to each other in the Hubbard model. The error in the self-consistent spin-polarized Kohn-Sham DFT HSE06 functional is much larger than the usual 0.1 eV [22]. Our Hubbard model Hamiltonian derivation clearly shows that the ${}^1B_1$ state is a particularly highly correlated multiplet which cannot be properly treated by Kohn-Sham hybrid density functionals.

TABLE II. HSE06 total energies of considered states of neutral N_2V relative to that of Ψ_1 obtained by fixed orbital calculation from the double negatively charged N_2V basis states in the optimized geometry of the neutral N_2V by the self-consistent spin-polarized HSE06 calculation. We note that the chosen relative energies correspond to an energy shift of $\frac{t-U-C-3J}{2}$ in (H') [see Eq. (2)].

State	Relative energy (eV)
Ψ_1	0.00
Ψ_2	1.01
Ψ_3	2.23
${}^3B_1$	−0.05

V. *AB INITIO* MAGNETO-OPTICAL PARAMETERS

For direct comparison to the experimental ZPL data, one has to calculate the relaxation energy of ions upon excitation. The relaxation energy was very roughly estimated by self-consistent spin-polarized HSE06 ΔSCF method on Ψ_{1-3} states. We find that the relaxation energy on the ${}^1A_{1(e)}$ state is ≈0.6 eV whereas it is ≈0.2 eV on the ${}^1B_1$ state. The relaxation energy on ${}^3B_1$ is small, 0.06 eV. The final results are depicted in Fig. 3 that are directly compared to experimental data and the self-consistent spin-polarized Kohn-Sham HSE06 results. Our Hubbard model Hamiltonian with *ab initio* parameters provides significantly improved results over those obtained by the usual self-consistent unrestricted spin-polarized Kohn-Sham HSE06 method. We find that the ${}^1A_{1(g)} \to {}^1B_1$ ZPL energy is indeed around 2.4 eV, and the ${}^1A_{1(g)} \to {}^1A_{1(e)}$ ZPL energy is slightly above that. These are the optically allowed transitions. Higher energy singlet and triplet states with $b_2 \to b_1$ excitation may form with optically forbidden A_2 symmetry. The ${}^1A_2$ state cannot absorb light but can play a role in the nonradiative decay when the electron is excited to the H13 band which corresponds to the valence band to b_1 transition (see Fig. 3). The total energy of the ${}^3A_2$ could be a calculated ΔSCF procedure from ${}^3B_1 \to {}^3A_2$ excitation energy whereas the total energy of ${}^1A_2$ should be slightly higher due to the small singlet-triplet coupling J.

Regarding the triplet energy levels, their energies in the region of 270–480 meV below the ${}^1B_1$ level were proposed from PL lifetime measurements where they found a delayed luminescence of millisecond lifetime [11] that they associated with a spin-orbit mediated tunneling process [33] from the metastable triplets to the lowest energy singlet excited state with the formula

$$W(T) = \frac{K}{\sqrt{kT^*}} \coth\left(\frac{\hbar\omega}{2kT}\right) \exp\left(-\frac{E_a}{kT^*}\right), \tag{4}$$

$$K = \frac{|C_{sl}|^2 \omega \sqrt{2\pi}}{\sqrt{2E_M}}, \tag{5}$$

$$C_{sl} = \frac{\langle s|\hat{H}_{\mathrm{SO}}|l\rangle J_{sl}}{E_s - E_l}, \tag{6}$$

with $kT^* = \frac{1}{2}\hbar\omega \coth(\hbar\omega/2kT)$, E_a is the barrier energy between the corresponding states, $\hbar\omega$ is the dominant phonon

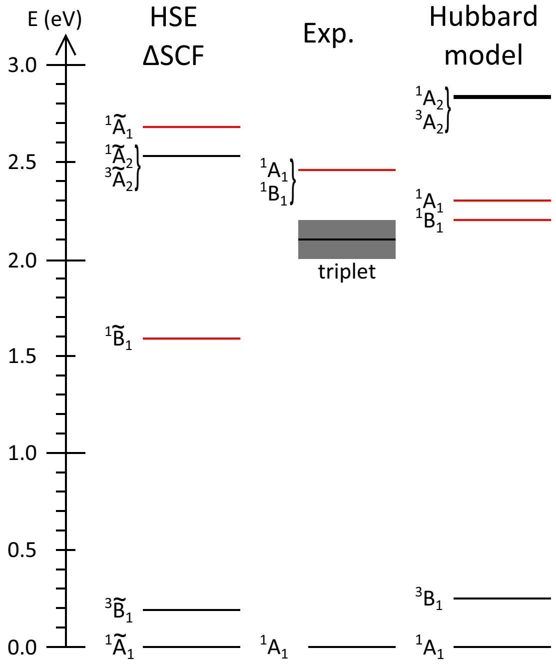

FIG. 3. Excitation energies of the neutral N_2V defect in diamond. States that are very close in energy are enclosed with brackets. The lowest optically allowed excitation energies are highlighted with red. Left panel: self-consistent unrestricted spin-polarized Kohn-Sham HSE06 ΔSCF results. The tilde on the labels of the wave functions denotes that not the true eigenstate of the system is calculated (see text for more details). Middle panel: experimental zero-phonon-line energies for the singlets (Ref. [7]) and the proposed energies of triplets (Ref. [11]). Right panel: Hubbard model Hamiltonian results.

frequency, E_M is the relaxation energy between the two states, k is the Boltzmann constant, and T is the temperature in K. C_{sl} is the coupling of states s and l where $\hat{H}_{\mathrm{SO}}$ is the spin-orbit coupling operator; J_{sl} is the electron-phonon coupling. We found that the $^3B_1$ level is rather far (>2 eV) from the excited singlet states, thus we estimated its delayed luminescence. As the transition from $^3B_1$ to $^1B_1$ is a second-order process which should be presumably slow, we calculated the transition to $^1A_1$ with the first-order ISC process. The estimated strength of spin-orbit coupling is around 10 GHz and that of the electron-phonon coupling is $0.1\sqrt{\mathrm{eV}}$, similar to the values in the NV center [34,35]. From our vibrational analysis, calculated with the computationally less expensive PBE functional [36] using PBE optimized geometries, we obtained the average phonon energy of 84 meV weighted by the partial Huang-Rhys factors [37] for the vibrational coupling for this transition. The relaxation energy between $^1A_1$ and $^3B_1$ is estimated to be 0.4 eV. With these parameters we obtain a lifetime in the order of 10^6 s at various temperatures. This implies that the observed delayed luminescence is not intrinsic to the defect. As the delayed luminescence was observed for the ensemble of N_2V defects we speculate that it originates from the interaction with other defects in diamond. Future single defect measurements may conclude the nature of this emission.

In the following, we present the calculated hyperfine interaction of the electron spin with ^{14}N and proximate ^{13}C nuclear spins. The identification of ^{13}C sites with dominant hyperfine parameters in the vicinity of N_2V defect is of great importance in quantum memory realization with this defect as they can store the quantum information for a relatively long time. These sites are highlighted in Fig. 4 and the corresponding calculated hyperfine parameters are listed in Table III.

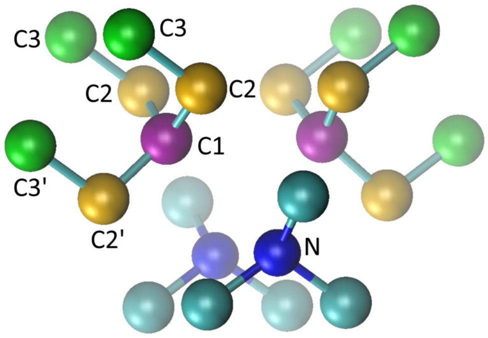

FIG. 4. Visualization of atomic sites with dominant hyperfine parameters shown in Table III for N_2V^0.

VI. SUMMARY

We analyzed the neutral N_2V defect in diamond by means of *ab initio* calculations, and concluded that a quantum memory can be realized by this defect controlled by optical excitation and microwave manipulation. We showed that the electronic structure of this defect is a prototype of highly correlated states that can be treated by our method that is a combination of density functional theory and a Hubbard model.

ACKNOWLEDGMENT

We acknowledge the support from EU Commission on the DIADEMS project (Contract No. 611143).

APPENDIX A: ADDITIONAL FORMULAS FOR THE HUBBARD MODEL

In this section, we explicitly show the connection between the DFT total energies of the single determinant states and the multiplets, and write down the formulas that we applied

TABLE III. HSE DFT calculated hyperfine constants for N_2V^0 for ^{14}N and ^{13}C nuclei. The location of ^{13}C nuclei is depicted in Fig. 4.

Site	A_{xx} (MHz)	A_{yy} (MHz)	A_{zz} (MHz)
^{14}N	9.6	9.5	14.5
C1	82.3	81.7	198.9
C2	−11.5	−8.5	−12.1
C2’	−11.2	−8.3	−11.6
C3	15.9	15.7	24.2
C3’	16.1	15.9	24.4

TABLE IV. HSE06 total energies of considered states of neutral N_2V relative to that of ${}^1\tilde{A}_{1(g)}$ are obtained by self-consistent unrestricted spin-polarized HSE06 calculation in the optimized geometry of the neutral N_2V. The tilde over the electronic states labels that those states are not the true symmetrical eigenstates of the system.

State	Relative energy (eV)
${}^1\tilde{A}_{1(g)}$	0.00
${}^1\tilde{B}_1$	1.67
${}^1\tilde{A}_{1(e)}$	2.92
${}^3\tilde{B}_1$	0.25

to obtain the Hubbard parameters and calculate the excitation energies.

By using the definitions of *a* and *b* orbitals in the main text, one can express the corresponding wave functions in terms of *A* and *B* dangling bonds as

$$|{}^1A_{1(g)}\rangle = \tfrac{1}{2}(|A^\uparrow A^\downarrow\rangle + |B^\uparrow B^\downarrow\rangle) + \tfrac{1}{2}(|B^\uparrow A^\downarrow\rangle - |B^\downarrow A^\uparrow\rangle), \tag{A1}$$

$$|{}^1A_{1(e)}\rangle = \tfrac{1}{2}(|A^\uparrow A^\downarrow\rangle + |B^\uparrow B^\downarrow\rangle) - \tfrac{1}{2}(|B^\uparrow A^\downarrow\rangle - |B^\downarrow A^\uparrow\rangle), \tag{A2}$$

$$|{}^1B_1\rangle = \frac{1}{\sqrt{2}}(|A^\uparrow A^\downarrow\rangle - |B^\uparrow B^\downarrow\rangle), \tag{A3}$$

$$|{}^3B_1\rangle = \begin{cases} |A^\uparrow B^\uparrow\rangle \\ \frac{1}{\sqrt{2}}(|B^\uparrow A^\downarrow\rangle + |B^\downarrow A^\uparrow\rangle) \\ |A^\downarrow B^\downarrow\rangle \end{cases}. \tag{A4}$$

By applying the Hubbard Hamiltonian in the main text, one obtains Hamiltonian matrix in the basis of $|{}^1A_{1(g)}\rangle$, $|{}^1A_{1(e)}\rangle$, $|{}^1B_1\rangle$, $|{}^3B_1\rangle$ as shown in the main text. After diagonalization of the Hubbard Hamiltonian, the resultantt vertical excitation energies are

$$E({}^1A_{1(g)} \to {}^1A_{1(e)}) = \sqrt{t^2 + (U - C - 3J)^2}, \tag{A5}$$

$$E({}^1A_{1(g)} \to {}^1B_1) = \frac{U - C - 3J + \sqrt{t^2 + (U - C - 3J)^2}}{2}, \tag{A6}$$

$$E({}^1A_{1(g)} \to {}^3B_1) = \frac{C - U - 5J + \sqrt{t^2 + (U - C - 3J)^2}}{2}. \tag{A7}$$

TABLE V. Vertical excitation energies in the Hubbard model calculated from self-consistent unrestricted spin-polarized HSE06 Kohn-Sham orbitals.

Excitation	Vertical excitation energy (eV)
${}^1A_{1(g)} \to {}^3B_1$	1.07
${}^1A_{1(g)} \to {}^1B_1$	3.91
${}^1A_{1(g)} \to {}^1A_{1(e)}$	4.39

APPENDIX B: ADDITIONAL INFORMATION ABOUT THE RAW DFT TOTAL ENERGIES

We show in Table V that calculation of the total energies in the Hubbard model from unrestricted spin-polarized Kohn-Sham DFT HSE06 orbitals is not appropriate.

The total energy of ${}^1\tilde{A}_{1(g)}$ relative to that of Ψ_1 is -6.75 eV as listed in Table IV because we applied restriction to the Kohn-Sham orbitals as explained in the main text. The calculated excitation energies within the Hubbard model taking the values in Table IV are given in Table V. These results are very far from the experimental data. This can be understood by considering the fact that the unrestricted spin-polarized HSE06 Kohn-Sham orbitals are spin contaminated and *break* the symmetry of the system. Thus, these orbitals are not suitable for serving as a basis for the Hubbard model as the Hubbard model requires orbitals with appropriate symmetry and spin state.

[1] J. E. Field, *The Properties of Diamond* (Academic, London, 1976).

[2] G. Davies and M. F. Hamer, Proc. R. Soc. London, Ser. A **348**, 285 (1976).

[3] A. Mainwood, Phys. Rev. B **49**, 7934 (1994).

[4] G. Davies, J. Phys. C **9**, L537 (1976).

[5] J. Lowther, J. Phys. Chem. Solids **45**, 127 (1984).

[6] R. Jones, P. R. Briddon, S. Öberg, and V. J. Torres, in *Defects in Semiconductors 17*, Materials Science Forum Vol. 143 (Trans Tech Publications, Zürich, 1993), pp. 45–50.

[7] G. Davies, M. H. Nazare, and M. F. Hamer, Proc. R. Soc. London, Ser. A **351**, 245 (1976).

[8] M. D. Crossfield, G. Davies, A. T. Collins, and E. C. Lightowlers, J. Phys. C **7**, 1909 (1974).

[9] J.-H. Hsu, W.-D. Su, K.-L. Yang, Y.-K. Tzeng, and H.-C. Chang, Appl. Phys. Lett. **98**, 193116 (2011).

[10] A. T. Collins, J. Phys. C **16**, 6691 (1983).

[11] E. Pereira and T. Monteiro, J. Lumin. **48**, 814 (1991).

[12] J. A. van Wyk and G. S. Woods, J. Phys.: Condens. Matter **7**, 5901 (1995).

[13] A. Gruber, A. Dräbenstedt, C. Tietz, L. Fleury, J. Wrachtrup, and C. von Borczyskowski, Science **276**, 2012 (1997).

[14] S.-Y. Lee, M. Widmann, T. Rendler, M. W. Doherty, T. M. Babinec, S. Yang, M. Eyer, P. Siyushev, B. J. M. Hausmann, M. Loncar, Z. Bodrog, A. Gali, N. B. Manson, H. Fedder, and J. Wrachtrup, Nat. Nanotechnol. **8**, 487 (2013).

[15] U. von Barth, Phys. Rev. A **20**, 1693 (1979).

[16] J. Heyd, G. E. Scuseria, and M. Ernzerhof, J. Chem. Phys. **118**, 8207 (2003).

[17] P. E. Blöchl, Phys. Rev. B **50**, 17953 (1994).

[18] G. Kresse and J. Hafner, Phys. Rev. B **47**, 558 (1993).

[19] G. Kresse and J. Furthmüller, Phys. Rev. B **54**, 11169 (1996).

[20] G. Kresse and J. Furthmüller, Comput. Mater. Sci. **6**, 15 (1996).

[21] J. Paier, M. Marsman, K. Hummer, G. Kresse, I. C. Gerber, and J. G. Ángyán, J. Chem. Phys. **124**, 154709 (2006).
[22] P. Deák, B. Aradi, M. Kaviani, T. Frauenheim, and A. Gali, Phys. Rev. B **89**, 075203 (2014).
[23] M. Kaviani, P. Deák, B. Aradi, T. Frauenheim, J.-P. Chou, and A. Gali, Nano Lett. **14**, 4772 (2014).
[24] K. Szász, T. Hornos, M. Marsman, and A. Gali, Phys. Rev. B **88**, 075202 (2013).
[25] V. Ivády, T. Simon, J. R. Maze, I. A. Abrikosov, and A. Gali, Phys. Rev. B **90**, 235205 (2014).
[26] B. L. Green, M. W. Dale, M. E. Newton, and D. Fisher, Phys. Rev. B **92**, 165204 (2015).
[27] V. Ivády, K. Szász, A. L. Falk, P. V. Klimov, D. J. Christle, E. Janzén, I. A. Abrikosov, D. D. Awschalom, and A. Gali, Phys. Rev. B **92**, 115206 (2015).
[28] V. Ivády, P. V. Klimov, K. C. Miao, A. L. Falk, D. J. Christle, K. Szász, I. A. Abrikosov, D. D. Awschalom, and A. Gali, Phys. Rev. Lett. **117**, 220503 (2016).
[29] V. Jacques, P. Neumann, J. Beck, M. Markham, D. Twitchen, J. Meijer, F. Kaiser, G. Balasubramanian, F. Jelezko, and J. Wrachtrup, Phys. Rev. Lett. **102**, 057403 (2009).
[30] A. S. Zyubin, A. M. Mebel, M. Hayashi, H. C. Chang, and S. H. Lin, J. Phys. Chem. C **113**, 10432 (2009).
[31] J. Hubbard, Proc. R. Soc. London, Ser. A **276**, 238 (1963).
[32] A. Gali, E. Janzén, P. Deák, G. Kresse, and E. Kaxiras, Phys. Rev. Lett. **103**, 186404 (2009).
[33] K. F. Freed and J. Jortner, J. Chem. Phys. **52**, 6272 (1970).
[34] A. Batalov, V. Jacques, F. Kaiser, P. Siyushev, P. Neumann, L. J. Rogers, R. L. McMurtrie, N. B. Manson, F. Jelezko, and J. Wrachtrup, Phys. Rev. Lett. **102**, 195506 (2009).
[35] G. Thiering and A. Gali, Phys. Rev. B **96**, 081115(R) (2017).
[36] J. P. Perdew, K. Burke, and M. Ernzerhof, Phys. Rev. Lett. **77**, 3865 (1996).
[37] K. Huang and A. Rhys, Proc. R. Soc. London, Ser. A **204**, 406 (1950).